THE JOURNAL OF PHYSICAL CHEMISTRY B

ARTICLE

pubs.acs.org/JPCB

# Comparative Study of Direct and Phase-Specific Vibrational Sum-Frequency Generation Spectroscopy: Advantages and Limitations

Ruben E. Pool,[†] Jan Versluis,[†] Ellen H. G. Backus,[†] and Mischa Bonn*[,†,‡]

[†]Fom Institute AMOLF, P.O. Box 41883, 1009 DB Amsterdam, Netherlands

[‡]Max-Planck Institute for Polymer Research, Ackermannweg 10, 55128 Mainz, Germany

**ABSTRACT:** As a surface-specific technique, vibrational sum-frequency generation (SFG) is used in a wide range of applications where soft matter or solid interfaces are to be probed on a molecular level through their vibrational modes. In recent years, phase-specific sum-frequency generation (PS-SFG, also known as heterodyne-detected SFG) spectroscopy has been increasingly replacing its predecessor (direct SFG, also known as homodyne SFG) as the experimental technique of choice for characterizing interfacial structure. The technique enables phase sensitive measurements, allowing for the determination of the real and imaginary parts of the interfacial vibrational response function and thereby the unambiguous identification of molecular orientation. This phase-sensitivity requires, however, a complete understanding of the complex optical properties of the sample and of their effect on the signal. These optical properties significantly influence the raw spectral data from which the real and imaginary parts of the second-order susceptibility are retrieved. We show that it is essential to correct the data appropriately to infer the true molecular response. The current study presents a detailed description of the physical contributions to the phase-resolved spectrum, allowing a direct comparison between the phase-resolved spectrum and that obtained using the well-understood direct detection method in a step-by-step data analysis process. In addition to phase sensitivity, PS-SFG has been shown to increase the sensitivity compared to traditional (direct) SFG spectroscopy. We present a quantitative comparison between theoretical limits of the signal-to-noise ratio of both techniques, which shows that for many systems the signal-to-noise ratio is very similar for direct- and phase-specific SFG signals.

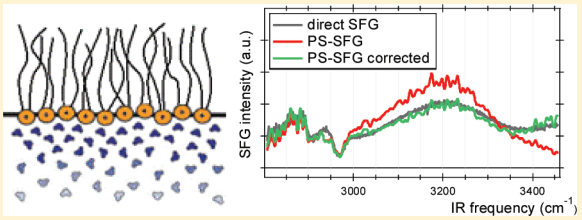


## INTRODUCTION

Vibrational sum frequency generation (SFG) spectroscopy is in many ways an ideal technique for probing the structure of interfaces at the molecular level. As with infrared spectroscopy, vibrational modes are interrogated by an infrared laser source of resonant frequency $\omega_1$ in order to identify the spectral signatures of the molecular moieties present. In SFG spectroscopy a second, non-resonant laser with (generally near-infrared) visible frequency $\omega_2$ is overlapped in time and space with the first one, upconverting the vibrational polarization into the visible region, through a virtual state. Emission from this state at frequency $\omega = \omega_1 + \omega_2$ lies well within the visible optical region and can therefore be detected background-free and sensitively by commercially available CCD cameras. The true strength of SFG spectroscopy, however, lies in the surface specificity of the technique. Since the instantaneous excitation and upconversion of molecular vibrations is a two-photon process, the intensity of the sum-frequency emission is determined by the second-order nonlinear susceptibility $\chi^{(2)}$ of the sample and the strength of the incoming visible and infrared fields:

$$I_{SFG} = |E_{SFG}|^2 \propto |\chi^{(2)} E_{VIS} E_{IR}|^2 \quad (1)$$

The molecular information contained in the detected SFG spectrum thus originates from $\chi^{(2)}$, being the macroscopic average of the molecular hyperpolarizability. For a centrosymmetric medium, which most bulk materials are, $\chi^{(2)}$ cancels out in the dipole approximation and no SFG signal is generated from the bulk. Only when the symmetry is broken, e.g., at an interface, the sum-frequency field becomes finite. It is this surface specificity that sets SFG spectroscopy apart from other infrared techniques by enabling detection of water, surfactants, and surface-bound peptides and proteins at the interface that would otherwise be indiscernible from the typically much larger bulk signal. For this reason the technique has become very popular since its first application approximately two decades ago.[1−9] On the other hand, it can be argued that SFG spectroscopy has not yet reached its full potential because of a lack of uniformity in the presentation of data: to extract $|\chi^{(2)}|^2$ from the detected intensity, corrections need to be made for the Fresnel factors that depend on the specific geometric of the setup, a practice that is not always explicitly described. The inconsistencies thus arising in spectra of, for example, the air−water interface were recently addressed and shown to be converging to an accepted standard.[10]

**Received:** August 17, 2011
**Revised:** November 9, 2011
**Published:** November 10, 2011





dx.doi.org/10.1021/jp2079023 | J. Phys. Chem. B 2011, 115, 15362–15369

A more fundamental shortcoming of the technique lies in the detection of the squared term $|\chi^{(2)}|^2$ (see eq 1), whereby all information on the complex nature of $\chi^{(2)}$ is lost. This drawback can be circumvented by the application of an interference-based phase-specific SFG (PS-SFG) detection scheme, as was initially demonstrated by the group of Shen,[11] and subsequently by several other groups.[12−14] With this approach one can obtain phase sensitive spectra. By mixing the sample signal with a local oscillator (LO) of known phase, the detected intensity contains not only the squared field strengths but also two cross terms:

$$I = |E_{det}|^2 = |E_{LO} + E_{sample}|^2$$
$$= |E_{LO}|^2 + |E_{sample}|^2 + E_{LO}E^*_{sample} + E^*_{LO}E_{sample} \quad (2)$$

From these cross terms, the complex $\chi^{(2)}$ can be extracted, as the cross terms contain the phase information of the resonances that is lost in more conventional direct SFG measurements. The imaginary part of $\chi^{(2)}$, $\mathrm{Im}[\chi^{(2)}]$, shows the vibrational resonances, and can be thus directly compared to what is measured in a linear IR absorption measurement. However, these resonant peaks can be either positive or negative in the $\mathrm{Im}[\chi^{(2)}]$ of an PS-SFG spectrum, and it is this phase of the vibration that is indicative of the direction of the aligned molecules, making it possible to distinguish "up"-pointing molecular bonds from "down"-pointing ones.[15] This additional information on interfacial molecular structure makes the potential of PS-SFG even larger than that of its direct counterpart, and promising results have been published using several forms of the technique.[11−14,16,17] Several authors have used the term '"heterodyne SFG" to indicate this novel technique and "homodyne" for the direct SFG approach. This nomenclature is technically not correct, since heterodyning implies interference with a local oscillator of a different frequency to frequency-shift the detected signal. PS-SFG is therefore strictly speaking a homodyne technique, but to avoid further confusion we refrain from using either term altogether, and refer here to phase-resolved and direct SFG.

The benefits of phase-resolved SFG come at a price: extracting the complex $\chi^{(2)}$ from the measured intensity spectrum is less straightforward than finding $|\chi^{(2)}|$.[2] In the latter case, only the Fresnel factors need to be corrected for, which determine the local field effects of IR, VIS and SFG field in dependence of the particular angles of incidence, polarizations, and the resulting phase matching conditions.[18] In the PS-SFG case however, additional corrections are needed to find the true real and imaginary parts of $\chi^{(2)}$. First, a z-cut quartz crystal is generally used as a nonresonant reference to obtain the infrared spectral shape. The use of such a reference is traditionally thought to require a correction of the complex phase of 90° because of the mismatch between the bulk-like response of the quartz reference and the surface-like response of aqueous interfaces,[19,20] although more recent measurements suggest a correction closer to 115°.[21] Further, in most experimental geometries, either the visible and infrared pulse generating the LO[13,14] or the LO itself[11,12] are reflected from the sample. The complex reflection coefficient of the sample (of water, for example) may greatly influence the spectral shape of both the SFG intensity and phase, as will be demonstrated below. Finally, a seemingly trivial but important source of phase aberrations originates from the challenge in maintaining phase stability of the experimental setup.

As a result of these challenges, there is no complete consistency between different phase-detected studies.[10,22] Specifically, details of the sign and the zero-crossing point of the imaginary spectrum have remained debated,[10,22] which may lead to varying interpretations of molecular structure at the interface. Apparently, the corrections described above for retrieving the complex $\chi^{(2)}$ from the phase-resolved measurements are not yet fully understood or universally applied.

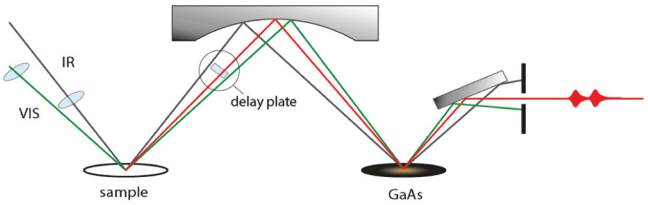


**Figure 1.** Experimental geometry of PS-SFG detection. Laser pulses in the 800 nm (VIS) and mid-infrared (IR) ranges are focused onto the aqueous interface of the sample, generating an SFG response that is delayed by a silica plate. The three beams are refocused by a spherical mirror onto a gallium arsenide (GaAs) wafer, generating a second SFG response that interferes with the sample signal on the CCD.

In this study, we present phase-resolved and direct measurements of lipid monolayers of positive and negative charge on water. We record the SFG spectra across the lipid CH and water OH resonances. We explicitly show all the steps of PS-SFG data analysis, including the application of the aforementioned corrections in amplitude and phase and compare direct SFG and PS-SFG measurements in order to show the implications of these corrections. In this way, we hope to promote reproducibility and consistency between the many results that are certain to come from PS-SFG spectroscopy.

## MATERIALS AND METHODS

The experimental setup used to perform PS-SFG measurements is largely based on that developed by the Tahara group.[13] A total of 1 mJ of the output of a regeneratively amplified Ti:sapphire system (Legend, Coherent, Inc.) producing ∼35 fs pulses centered at 800 nm is used to generate tunable mid-IR pulses using a home-built optical parametric amplifier and difference frequency generation unit. A total of 0.5 mJ of the amplifier output is spectrally narrowed to ∼25 $cm^{-1}$ using a Fabry−Perot etalon. The IR beam passes through a half wave plate and polarizer before being focused onto the sample together with the spectrally narrowed visible beam. A focal length of 50 mm and 200 mm are used in this reflection geometry, with angles of incidence of 40° and 45° with respect to the surface normal and a remaining power of 5 mW and 25 mW (IR and visible, respectively; see Figure 1). The SFG signal generated in this way passes through a silica delay plate (1 mm, with antireflection coating) and is refocused, together with the reflected IR and visible pulses, onto a 110 gallium arsenide wafer (GaAs, 110 cut, from which the LO is generated) by means of a gold-coated spherical mirror with a focal length of 50 mm.

The remaining 800 nm light is filtered out, and the SFG signal is passed through a polarizer and focused into a spectrograph (Acton, Princeton Instruments) in which it is dispersed, via a grating, and focused onto an electron multiplied charge coupled device (emCCD) camera (Newton, Andor). All spectra reported in this study were collected under the ssp polarization condition (s polarized sum frequency, s polarized visible, p polarized IR). All measurements were conducted at 23 °C. Direct SFG measurements were performed by blocking the IR between the sample and GaAs. Note that the reflectivity of GaAs is low in this geometry (<0.4), causing a significant loss in SFG signal

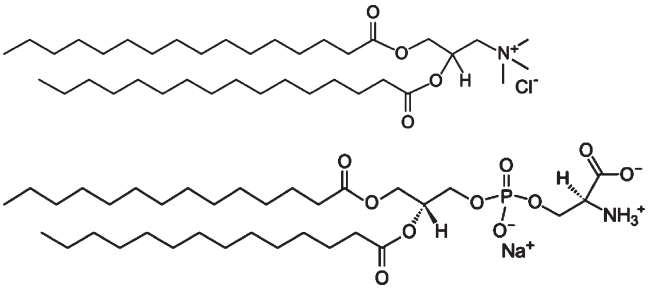

**Figure 2.** Chemical structures of DPTAP (top) and DMPS (bottom). Their net positive and negative charge will result in alignment of the water with hydrogen atoms down and up, respectively. It is this phase of the vibration that can be identified through PS-SFG spectroscopy.

strength. The reflection coefficient is, however, wavelength independent, ruling out the danger of spectral distortion.

To extract the true phase of $\chi^{(2)}$ from the PS-SFG measurements, the height and angular placement of the quartz reference and the aqueous sample have to be highly reproducible. To this end, a diode laser pointer was reflected off the sample site and projected in the far field onto a millimeter grid. Monitoring both the position of the reflected laser light on the grid and the position of the SFG signal on the CCD camera enabled a reproducibility of the phase of the quartz and lipid samples within 3°.

Cationic 1,2-dipalmitoyl-3-trimethylammonium-propane (DPTAP) and anionic 1,2-dimyristoyl-*sn*-glycero-3-phospho-L-serine (DMPS) were obtained from Avanti Polar Lipids; their chemical structures are shown in Figure 2. Self-assembled monolayers were produced by dropcasting a solution of this lipid in chloroform (1 g/L) drop by drop onto a pure $H_2O$ subphase. $H_2O$ used in this study was demineralised and then filtered using a Millipore unit to a final resistivity of 18 MΩ cm. Samples were prepared in a 70 mm × 70 mm Teflon-coated aluminum trough (approximately 20 mL). The experiments were performed at a surface pressure of 22 ± 2 mN/m, measured with a commercially available tensiometer (Kibron, Finland).

## EXPERIMENT AND ANALYSIS: AMPLITUDE AND PHASE CORRECTIONS

In broadband frequency-domain SFG spectroscopy, the nonlinear response of a surface is induced by overlapping a broadband infrared (IR) and a narrowband visible (VIS) pulse in both time and space. In PS-SFG spectroscopy, this signal is mixed with a local oscillator of independent phase. For instance, the reflected VIS and IR and the generated SFG beams can be refocused on a medium with a frequency independent (i.e., nonresonant) second-order nonlinear response, e.g., GaAs, on the surface of which the local oscillator (LO) is then generated. The detected field $E_{det}$ is the sum of the contribution from the LO ($E_{LO}$) and that of the sample ($E_{sample}$), reflected from the GaAs wafer:

$$E_{det} = E_{LO} + r_{GaAs}E_{sample} \tag{3}$$

where $r_{GaAs}$ is the reflection coefficient of the local oscillator medium.

The contributions of the sample and the LO are defined by the vacuum permittivity ($\varepsilon_0$), the geometry- and material-specific Fresnel factors ($F$), the second-order nonlinear susceptibility ($\chi^{(2)}$), and the incoming visible and IR fields ($E_{VIS}$ and $E_{IR}$), taking into account that these are reflected by the sample before reaching the GaAs:

$$E_{sample} = \varepsilon_0 F_{sample}\chi^{(2)}_{sample}E_{VIS}E_{IR}$$

$$E_{LO} = \varepsilon_0 F_{GaAs}\chi^{(2)}_{GaAs}r_{sample}(\omega_{VIS})r_{sample}(\omega_{IR})E_{VIS}E_{IR} \tag{4}$$

$\chi^{(2)}_{sample}$ is the quantity of interest, as it contains the molecular response and we aim to extract this quantity from the collected spectrum. Therefore, we focus below on canceling out the other factors. Keeping in mind that $E_{LO}$ is dependent on the incoming infrared and visible field and therefore on the reflectivity of the sample, it will be referred to as $E_{LO,s}$; this quantity differs from the local oscillator field obtained if the incident infrared and visible beams had not been first reflected off the sample. To obtain the spectral shape of the original IR excitation pulse required for the normalization of the sample spectrum, the sample is replaced by quartz, which is also a nonresonant material and gives a response $E_{quartz}$. The LO that is generated after reflection of the IR and VIS on quartz shall be referred to as $E_{LO,q}$.

The detected intensity is the square of the sum of all field strength contributions. In direct SFG spectroscopy only the sample field $E_{sample}$ contributes, causing the signal to be squared in its entirety and thereby losing all phase information. In PS-SFG spectroscopy, phase information is preserved within the linear cross-terms of the intensity of a signal composed of contributions of several sources (eq 2). These cross terms are extracted from the total intensity by introducing a controllable delay between the SFG response of the sample and that of the LO, as is explained below.

According to Fourier theory, a delay $\Delta t$ of the SF response of the sample relative to that of the LO results in an exponential prefactor in the frequency domain:

$$E_{det}(t) = E_{LO}(t) + r_{GaAs}E_{sample}(t-\Delta t) \rightarrow$$

$$E_{det}(\omega) = E_{LO}(\omega) + r_{GaAs}E_{sample}(\omega)e^{i\omega\Delta t} \tag{5}$$

With this delay, the intensity spectrum detected on the CCD camera is given by

$$\begin{aligned} I = |E_{det}|^2 &= |E_{LO} + r_{GaAs}E_{sample}e^{i\omega\Delta t}|^2 \\ &= |E_{LO}|^2 + |r_{GaAs}E_{sample}|^2 \\ &\quad + E_{LO}r^*_{GaAs}E^*_{sample}e^{-i\omega\Delta t} + E^*_{LO}r_{GaAs}E_{sample}e^{i\omega\Delta t} \end{aligned} \tag{6}$$

In Figure 3 this composed intensity is shown for a quartz reference and lipid (DPTAP) monolayer sample. The exponential delay term gives rise to fringes on the spectrum. They are much smaller for the sample than for quartz, displaying that the quartz response is of comparable size to the LO, whereas the response of this aqueous interface is much smaller. Linear terms are extracted from this composed intensity spectrum by taking the inverse Fourier transform (using an IFFT algorithm), resulting in a time-domain spectrum with the sum of the two quadratic terms at $t = 0$ and the two delayed terms on either side of this peak (Figure 4). The delayed term at $t = 1.6$ ps contains the unaltered $E_{sample}$ whereas the term at $t = -1.6$ contains its complex conjugate; these are the fourth and third terms, respectively, of the right-hand side of eq 6. The positively delayed term is selected by setting the values of the Fourier transforms outside the window shown in Figure 4 to zero and transforming back to the frequency domain by taking the

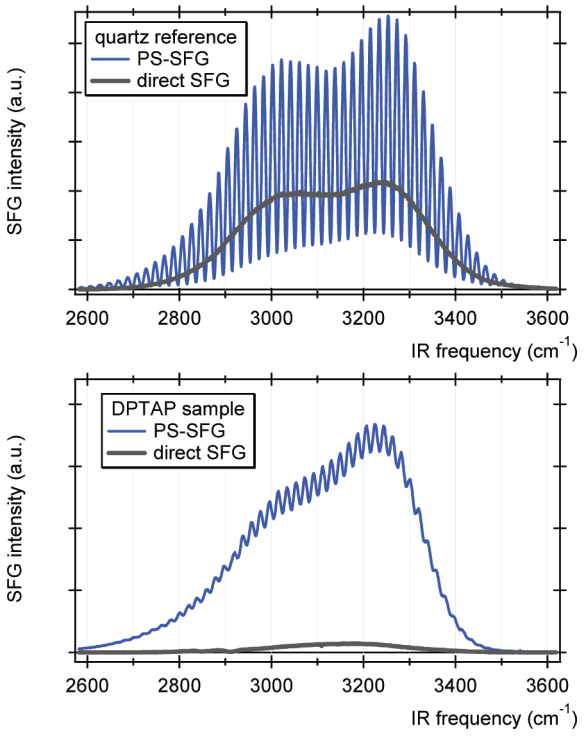


**Figure 3.** Intensity spectra of the quartz reference (top) and sample, a DPTAP monolayer on water (bottom). The quartz reference has an SFG response that is comparable in magnitude to the local oscillator in the PS-SFG measurements, causing strong interference and thus deep fringes. The lipid sample signal is much lower than the local oscillator, as can be seen by the narrow fringes. The direct SFG sample signal is 2 orders of magnitude smaller.

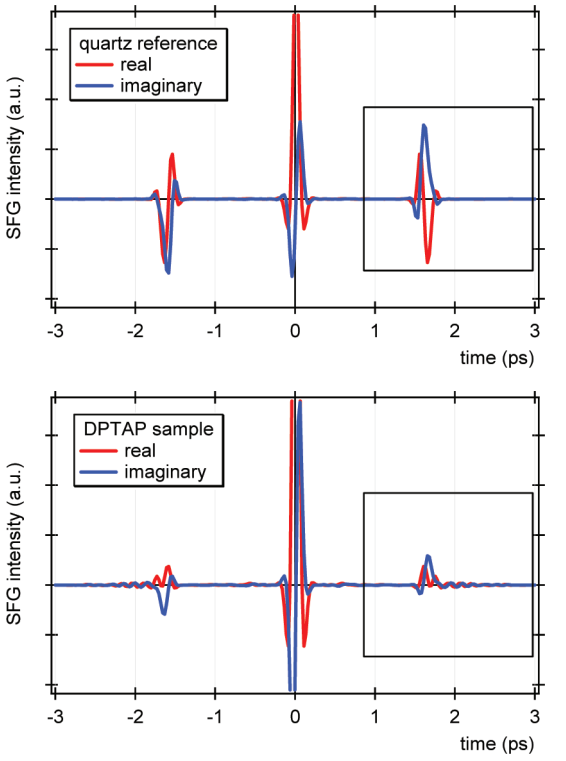


**Figure 4.** Inverse Fourier transforms of the spectra shown in Figure 3 (top quartz, bottom DPTAP sample). The sum of the two quadratic terms of eq 6 at $t = 0$ are flanked by the two delayed cross terms at $-\Delta t$ and $\Delta t$. The framed area shows the window of data that is selected; that is, all other values are set to zero before Fourier-transforming back to the frequency domain.

Fourier transform. We are left with the complex cross term, shown graphically and algebraically in Figure 5.

If we consider the two terms shown in Figure 5, it is evident that dividing these two terms cancels out the exponential term introduced by the delay and the reflection coefficient of the local oscillator. What we are then left with is one of the two linear cross terms from the total detected intensity (eq 6) normalized to account for the spectral shape of the IR excitation. In analogy with normalized direct SFG spectra, we may refer to this quantity as the extracted PS-SFG intensity $I_{PS}$

$$I_{PS} \equiv \frac{E^*_{LO,s} r_{GaAs} E_{sample} e^{i\omega\Delta t}}{E^*_{LO,q} r_{GaAs} iE_{quartz} e^{i\omega\Delta t}} = \frac{E^*_{LO,s} E_{sample}}{E^*_{LO,q} iE_{quartz}} \quad (7)$$

Note that we have also inserted a factor $i$ here to account for the 90° phase difference between the SFG response of the aqueous interface of the sample and the quartz crystal,[19,20] noting that the exact value of this correction is under debate.[10,21] Substituting eq 4 into this expression results in:

$$\begin{aligned} &\frac{E^*_{LO,s} E_{sample}}{iE^*_{LO,q} E_{quartz}} \\ &= \left(\frac{\varepsilon_0 F_{GaAs}\chi^{(2)}_{GaAs} r_{sample}(\omega_{VIS}) r_{sample}(\omega_{IR}) E_{VIS} E_{IR}}{\varepsilon_0 F_{GaAs}\chi^{(2)}_{GaAs} r_{quartz}(\omega_{VIS}) r_{quartz}(\omega_{IR}) E_{VIS} E_{IR}}\right)^* \frac{\varepsilon_0 F_{sample}\chi^{(2)}_{sample} E_{VIS} E_{IR}}{i\varepsilon_0 F_{quartz}\chi^{(2)}_{quartz} E_{VIS} E_{IR}} \\ &= \left(\frac{r_{sample}(\omega_{VIS}) r_{sample}(\omega_{IR})}{r_{quartz}(\omega_{VIS}) r_{quartz}(\omega_{IR})}\right)^* \frac{F_{sample}\chi^{(2)}_{sample}}{iF_{quartz}\chi^{(2)}_{quartz}} \end{aligned} \quad (8)$$

Clearly, all terms cancel out except for the reflection coefficients $r$, the Fresnel factors $F$ and the second-order nonlinear susceptibilities $\chi$, each of them different for the sample than for quartz. Since quartz is nonresonant, $\chi^{(2)}_{quartz}$ is constant (i.e., frequency independent), and $\chi^{(2)}_{sample}$ can be extracted from this expression by inserting $r$ and $F$. Traditionally, for direct SFG spectra a correction for $F$ is rarely made, that is, the presented direct SFG spectra are often not corrected for the Fresnel factors; if we proceed with the PS-SFG spectra along the same line, only the reflectivity of the sample and of quartz have to be considered. To show that we are indeed able to extract $F_{sample}\chi^{(2)}_{sample}$ correctly by means of this procedure, we compare $|F_{sample}\chi^{(2)}_{sample}|^2$ acquired by direct detection with the magnitude squared of $F_{sample}\chi^{(2)}_{sample}$ as obtained by PS-SFG. Let us briefly review the direct detection case, where the detected field is simply $E_{sample}$, and the detected intensity after normalization by the quartz reference is given by

$$I_{direct} = \frac{|E_{sample}|^2}{|E_{quartz}|^2} = \frac{|\varepsilon_0 F_{sample}\chi^{(2)}_{sample} E_{VIS} E_{IR}|^2}{|\varepsilon_0 F_{quartz}\chi^{(2)}_{quartz} E_{VIS} E_{IR}|^2} = \frac{|F_{sample}\chi^{(2)}_{sample}|^2}{|F_{quartz}\chi^{(2)}_{quartz}|^2} \quad (9)$$

To allow a quantitative comparison between the squared direct SFG terms to the linear PS-SFG spectrum, the squared magnitude of the latter should be taken

$$|I_{PS}|^2 = \frac{|E^*_{LO,s} E_{sample}|^2}{|E^*_{LO,q} E_{quartz}|^2} = \frac{|r_{sample}(\omega_{VIS}) r_{sample}(\omega_{IR})|^2}{|r_{quartz}(\omega_{VIS}) r_{quartz}(\omega_{IR})|^2} \frac{|F_{sample}\chi^{(2)}_{sample}|^2}{|F_{quartz}\chi^{(2)}_{quartz}|^2} \quad (10)$$


dx.doi.org/10.1021/jp2079023 |J. Phys. Chem. B 2011, 115, 15362–15369

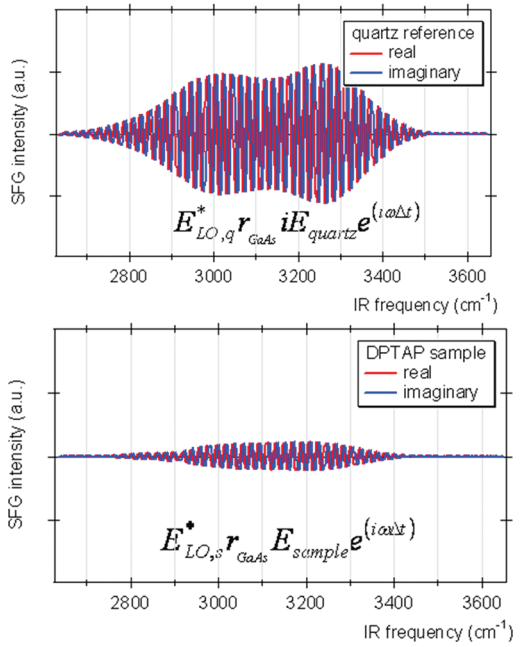


**Figure 5.** Linear terms of the PS-SFG intensity of the quartz reference (top) and DPTAP sample (bottom) obtained by Fourier transforming the selected regions of Figure 4. Dividing sample by reference gives what may be defined as the PS-SFG intensity $I_{PS}$, the normalized cross term of the total PS-SFG intensity (eq 7).

producing the relation

$$I_{\text{direct}} = \frac{|F_{\text{sample}}\chi^{(2)}_{\text{sample}}|^2}{|F_{\text{quartz}}\chi^{(2)}_{\text{quartz}}|^2} = \frac{|r_{\text{quartz}}(\omega_{\text{VIS}})r_{\text{quartz}}(\omega_{\text{IR}})|^2}{|r_{\text{sample}}(\omega_{\text{VIS}})r_{\text{sample}}(\omega_{\text{IR}})|^2}|I_{\text{PS}}|^2 \approx \frac{|r_{\text{quartz}}(\omega_{\text{IR}})|^2}{|r_{\text{sample}}(\omega_{\text{IR}})|^2}|I_{\text{PS}}|^2 \quad (11)$$

This indicates that a correction for the reflection coefficient should be sufficient to match the two spectra. In the last step we make use of the fact that the reflection coefficient is roughly frequency independent across the narrow bandwidth of the VIS pulse, so that we only have to consider the IR range. Also, it is safe to assume that the reflectivity of the water−lipid−air interface does not deviate much from that of the water−air interface, since only a single molecular layer of lipids is present.[23] The reflectivity of water has strong real and imaginary components in the mid-infrared, the latter due to its vibrational resonance, while the reflectivity of quartz is real, small and nonresonant, rendering its contribution to the signal negligible.

The reflectivity coefficient for the p-polarized infrared radiation is given by[24]

$$R_p = \left(\frac{n_1 \cos\vartheta_t - n_2 \cos\vartheta_i}{n_1 \cos\vartheta_t + n_2 \cos\vartheta_i}\right)^2 = \left(\frac{n_1\sqrt{1-\left(\frac{n_1}{n_2}\sin\vartheta_i\right)^2} - n_2\cos\vartheta_i}{n_1\sqrt{1-\left(\frac{n_1}{n_2}\sin\vartheta_i\right)^2} + n_2\cos\vartheta_i}\right)^2 \quad (12)$$

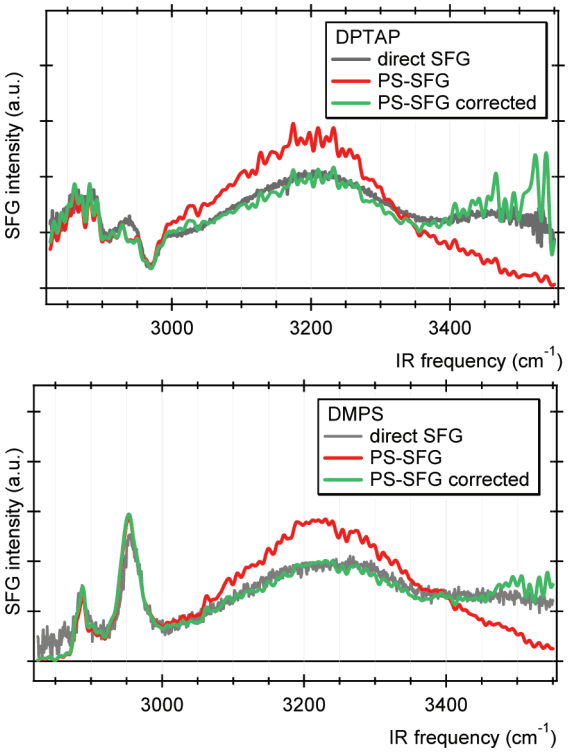


**Figure 6.** Intensity spectra of DPTAP (top) and DMPS (bottom) obtained by direct SFG and PS-SFG detection. The squared magnitude of the PS-SFG results is plotted, before and after correction for reflection coefficients. This correction does not cause much change in the CH region (the two peaks around 2900 cm$^{-1}$). The spectral shape of the broad OH band, however, is greatly affected by the reflection coefficients and only matches the direct SFG intensity spectrum after the correction is applied.

where $n_1$ is the index of refraction of air, $n_2$ the frequency-dependent complex index of refraction of water,[25] $\vartheta_t$ the angle of refraction, and $\vartheta_i$ the angle of incidence with respect to the surface normal. Note that in experiments where an isotopic dilution of $D_2O$ in $H_2O$ is used, determination of the reflection coefficient becomes more complex, since it is insufficient to consider a proportional combination of the index of refraction of both liquids, as the infrared response of HDO is not a linear combination of that of $D_2O$ and $H_2O$. As shown in the Appendix, there is also a reliable way of independently determining the squared magnitude of the reflectivity, which should be particularly helpful to assess the theoretical prediction of the reflection coefficient for such samples where the complex bulk refractive index is not confidently known.

In Figure 6, the effect of this correction is shown for a DPTAP and a DMPS monolayer. Both spectra show the $CH_3$ symmetric stretch (2880 cm$^{-1}$), the $CH_3$ Fermi resonance of the $CH_3$ symmetric stretch and bend overtone (2940 cm$^{-1}$), and the OH stretch (around 3200−3400 cm$^{-1}$) vibrations, while the DPTAP spectrum also displays the $CH_3$ antisymmetric stretch vibration as a dip at 2970 cm$^{-1}$; these are well-known from literature (e.g., ref 26). It is apparent that without correcting for the infrared reflectivity of the water interface there is significant disagreement between the direct SFG response and the "direct" response inferred from the PS-SFG measurements. Applying the mentioned correction for the reflection coefficient of water makes the direct SFG and PS-SFG spectra neatly overlap.

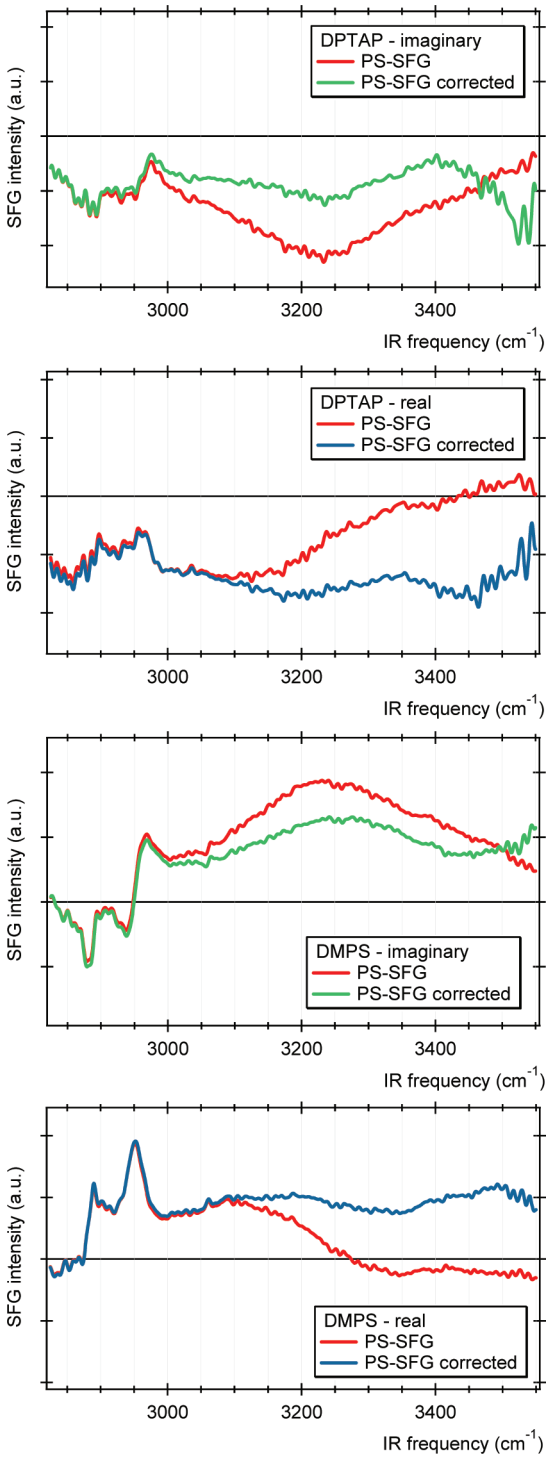


**Figure 7.** Imaginary and real parts of the complex spectra of DPTAP (top two panels) and DMPS (bottom two panels) found by PS-SFG detection and analysis. The results are shown before and after correction for the reflection coefficients, displaying the large influence of the sample reflectivity on the spectral shape.

The effect of the complex reflection coefficient correction on the imaginary and real part of $\chi^{(2)}$ is shown in Figure 7. The imaginary spectrum of DMPS reveals that here, too, the positive $CH_3$ antisymmetric stretch vibration is present at 2970 $cm^{-1}$, a feature that could not be identified in the direct SFG spectrum. The broad water peak is negative for DPTAP and positive for DMPS, in agreement with a study by the Tahara group.[16] Clearly, without the reflectivity correction the amplitude of the OH band in the Im$[\chi^{(2)}]$ spectrum is overestimated for both lipids, but the exact change in shape is dependent on the relative real and imaginary components. It seems evident that it is important to apply this correction before assigning individual resonances to the inferred spectral shape. Applying this correction can result in significant changes to amplitude, frequency and even sign of resonances. Note that above 3400 $cm^{-1}$ the reflection coefficient of water becomes very small, causing the noise on the corrected data to diverge. One should thus take care in considering this region in the fitting of the complex spectrum.

## DISCUSSION OF SNR

The preceding discourse shows that the correct interpretation of PS-SFG spectra hinges on careful data analysis and the application of corrections of the amplitude and phase of the signal. Provided these measures are taken, PS-SFG can provide complex spectra that contain the phase information of the studied interface, thereby surpassing the possibilities of direct SFG spectroscopy.

A second previously reported advantage arising from PS-SFG detection is an increase of signal-to-noise ratio (SNR).[12,13,17,27] Indeed, the PS-SFG signal can be orders of magnitude higher than the direct SFG signal due to interference with a large SFG signal from the local oscillator. Consequently, the detected PS-SFG signal may be lifted above noise sources in the detection, like dark current noise and read out noise. We show below that although the technique can provide a higher SNR in specific cases, it generally does not result in improvement. In order to quantify the increase in SNR we again compare direct SFG and PS-SFG detection. In this comparison we assume that the setup consists of state of the art experimental equipment. The direct SFG and PS-SFG noise terms consist of photon shot noise ($N_{shot}$), dark current noise ($N_{DC}$), and other noise sources in the readout (electrical, $N_R$). Hence the total noise in both measurements amounts to

$$N_{tot} = \sqrt{{N_{shot}}^2 + {N_{DC}}^2 + {N_R}^2} \tag{13}$$

In a typical direct SFG experiment, the photons are detected by a deep cooled (electron multiplying) charge coupled device [(em)CCD] camera. The number of detected SFG photons ranges from 1 to several thousand per pixel for a typical measurement.

For the camera that is used in our measurements, the dark current noise is 0.0002 counts per pixel per second and the read out noise amounts to 2.8 counts per pixel per read out. The dark current noise and readout noise of these instruments will therefore become irrelevant for data accquisitions ranging in the hundreds of counts per pixel. For the lipid monolayers studied in this paper, the intensity at resonances was 150 to 600 counts per pixel when setting an integration time of 360 s. When photon counts do indeed range in the hundreds, the SNR is dominated by photon shot noise, which scales with the square root of the total intensity. For the direct SFG measurements, we can then write the SNR as the ratio of the SFG intensity to the noise:

$$\mathrm{SNR}_{direct} = \frac{I_{sample}}{N_{tot}} \approx \frac{I_{sample}}{N_{shot}} \propto \frac{I_{sample}}{\sqrt{I_{sample}}} = \sqrt{I_{sample}}$$
$$N_{shot} > N_{DC}, N_R \tag{14}$$


dx.doi.org/10.1021/jp2079023 |J. Phys. Chem. B 2011, 115, 15362–15369

This relationship would imply that the larger signal $I$ observed in a PS-SFG measurement would result in increased signal-to-noise. The situation is not that simple, however: in a PS-SFG measurement, the SFG signal originates from multiple contributions, namely the SFG signal from the sample, the SFG signal from the local oscillator, and the cross terms (CT) due to interference of the two (eq 2). The cross term holds all the useful (phase) information and is proportional to the sample electric field ($E_{sample}$) times the local oscillator electric field ($E_{LO}$), but the signal is "carried" on top of the (generally) much larger signal from the local oscillator alone ($I_{LO}$).

Suppose that the field strength from the local oscillator is $c$ times higher than that emitted by the sample. The signal contributions are then given by

$$\begin{aligned} E_{LO} &= cE_{sample} \\ I_{LO} &= c^2 I_{sample} \\ I_{CT} &= E_{LO}E_{sample} = cE_{sample}{}^2 = cI_{sample} \end{aligned} \tag{15}$$

The total noise in the PS-SFG measurement consists of the combined noise from the sample, the local oscillator, and noise in the cross terms. Due to the strong signal from the local oscillator ($c \gg 1$), the total noise is dominated by the shot noise of this contribution

$$\begin{aligned} &N_{shot} \approx N_{shot,LO} \\ &N_{shot,LO} \propto \sqrt{I_{LO}} = cE_{sample} \quad c >> 1 \end{aligned} \tag{16}$$

The higher photon counts in the PS-SFG experiment lift the SFG signal above the dark current noise and electrical detection noise, which can also be neglected. Therefore in the PS-SFG experiment we only have to account for the photon shot noise from the local oscillator. The SNR for the PS-SFG signal is given by

$$\begin{aligned} &SNR_{PS} = \frac{I_{CT}}{N_{tot}} \approx \frac{I_{CT}}{N_{shot,LO}} \propto \frac{cI_{sample}}{cE_{sample}} = SNR_{direct} \\ &N_{shot} > N_{DC}, N_R \end{aligned} \tag{17}$$

Perhaps surprisingly, the SNR of the PS-SFG measurement is not sensitive to the signal strength of the local oscillator ($c$) and equals that of the direct SFG measurement in case the shot noise is the limiting factor. Analogous conclusions have been reached in the analysis of phase-sensitive second-harmonic generation spectroscopy.[28] Only if the SNR in the direct SFG measurement is not shot noise limited, i.e., if it is dominated by dark current noise or read out noise, an increase of SNR is expected in the PS-SFG measurement.

Furthermore, in the analysis we have assumed ideal experimental conditions for the PS-SFG experiment, with shot noise being the only source of noise. Figure 8 shows that under these conditions the SNR is equal for both techniques for all signal strengths (dashed line). In practice however, deviations from this ideal behavior will occur, as the GaAs is not a perfect reflector for the sample SFG signal. Therefore, a more realistic picture shows that PS-SFG does show an increase in SNR for low signal strengths due to lifting of the signal above dark current and read-out noise, while for higher numbers of counts direct SFG detection may be preferred, because of the PS-SFG signal loss caused by the GaAs reflectivity (Figure 8, solid lines). Another effect that realistically cannot be avoided is suboptimal interference: when the two fields $E_{sample}$ and $E_{LO}$ do not perfectly overlap on the CCD camera, the fringes caused by the interference will be less deep than theoretically possible, resulting in an overall lower intensity of the linear cross terms.[28] In Figure 8, these two effects, GaAs reflectivity and suboptimal interference, are assumed to lower the real PS-SFG SNR by a factor of 0.7 when compared to the ideal SNR. Note that extracting the PS-SFG cross term by selecting a time window (Figure 4) is a form of Fourier filtering, and in this process some high-frequency noise is filtered out. Since this practice is also possible for direct SFG spectra, it is not an intrinsic advantage of PS-SFG spectroscopy. One should take notice of this filtering effect when comparing direct SFG and PS-SFG spectra in the way that is shown in Figure 6, since the noise that is apparent in the spectrum may be misleading.

Summarizing this section on signal-to-noise, PS-SFG spectroscopy can reach a better SNR in the case of samples that generate very weak SFG fields, but generally PS-SFG detection

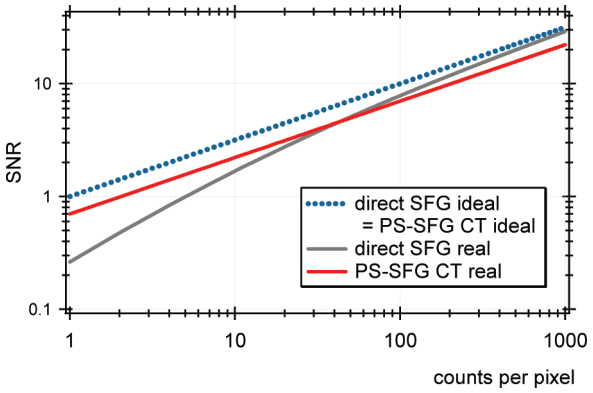


**Figure 8.** Theoretical predictions of direct SFG and PS-SFG signal-to-noise ratio (SNR) as a function of photon counts per pixel of the total spectrum (direct case) or of the cross term (CT, PS-SFG case). Although in the ideal case of only shot noise the two are equal (eq 17), realistically PS-SFG detection performs better at very low photon counts since the strong local oscillator intensity lifts the signal above the read-out noise. Alternatively, at higher photon counts the SNR of PS-SFG detection can be expected to be surpassed by direct detection because of the signal loss due to GaAs reflectivity and suboptimal interference.

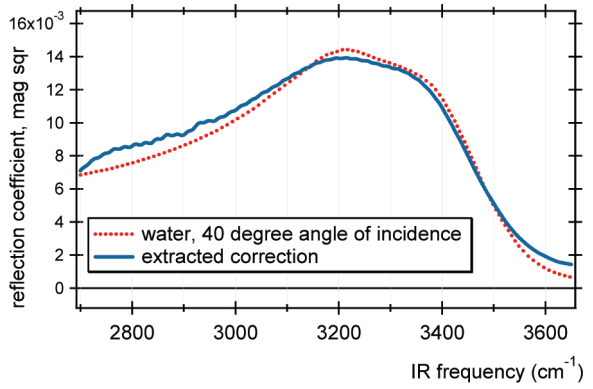


**Figure 9.** Squared magnitude of the sample reflectivity extracted from the quadratic terms of the PS-SFG intensity spectrum (eq 20) compared to the theoretical reflection coefficient of water (also magnitude squared). This method may be helpful to assess the reflectivity of samples of which the theoretical reflectivity is not straightforward to obtain, such as isotopic dilutions of $D_2O$ in $H_2O$.

does not result in improvement of the SNR for the case of the relatively high signals of a typical aqueous or metallic surface. The underlying reason is that, while overall signal levels are indeed increased for PS-SFG compared to direct detection, the shot noise also increases proportionally. While it is evident that implementing PS-SFG spectroscopy can overcome the sensitivity limits of the direct SFG technique in the very low signal limit, it is certainly not true that the SNR increases as a general rule.

## CONCLUSION

We have shown that with correct data analysis and reflectivity corrections, the PS-SFG and direct SFG signals can be equated. A particularly important correction originates from the fact that the spectrum of the infrared pulse at the local oscillator is different from that at the sample due to dispersion in the linear reflectivity of the sample. Our data show that correcting for this influences the shape of the retrieved second-order nonlinear susceptibility $\chi^{(2)}$ significantly, indicating that care must be taken when extracting the complex $\chi^{(2)}$ from the PS-SFG intensity spectra: without the proper correction, the spectra of the imaginary part of $\chi^{(2)}$ may contain features that do not reflect the physical reality of the surface. Additionally we have made a theoretical prediction of the signal-to-noise that can be obtained by PS-SFG, and show that generally the signal-to-noise of direct- and PS-SFG detected signals will be very similar when limited by shot noise; only at very low signal strengths will the signal-to-noise of PS-SFG detection exceed that of direct detection.

## APPENDIX: CALCULATED AND EMPIRICAL REFLECTIVITY CORRECTIONS

The magnitude squared reflectivity correction can be calculated, given the experimental geometry and the tabulated complex refractive index of the aqueous interface, but it can also be extracted from the squared terms of the total PS-SFG intensity

$$\begin{aligned}&|E_{\mathrm{LO,s}}|^2 + |r_{\mathrm{GaAs}}E_{\mathrm{sample}}|^2\\ &\quad = |\varepsilon_0 F_{\mathrm{GaAs}}\chi^{(2)}_{\mathrm{GaAs}} r_{\mathrm{sample}}(\omega_{\mathrm{VIS}}) r_{\mathrm{sample}}(\omega_{\mathrm{IR}}) E_{\mathrm{VIS}}E_{\mathrm{IR}}|^2\\ &\qquad + |r_{\mathrm{GaAs}}\varepsilon_0 F_{\mathrm{sample}}\chi^{(2)}_{\mathrm{sample}} E_{\mathrm{VIS}}E_{\mathrm{IR}}|^2\\ &\quad \approx |\varepsilon_0 F_{\mathrm{GaAs}}\chi^{(2)}_{\mathrm{GaAs}} r_{\mathrm{sample}}(\omega_{\mathrm{VIS}}) r_{\mathrm{sample}}(\omega_{\mathrm{IR}}) E_{\mathrm{VIS}}E_{\mathrm{IR}}|^2 \qquad (18)\end{aligned}$$

In the last step we use that $\chi^{(2)}_{\mathrm{sample}} \ll \chi^{(2)}_{\mathrm{GaAs}}$. In principle, the sample term can be canceled by subtracting the direct SFG spectrum from this expression, making it more precise.

For quartz, both terms are of comparable magnitude and cannot be simplified

$$\begin{aligned}&|E_{\mathrm{LO,q}}|^2 + |r_{\mathrm{GaAs}}E_{\mathrm{quartz}}|^2\\ &\quad = |\varepsilon_0 F_{\mathrm{GaAs}}\chi^{(2)}_{\mathrm{GaAs}} r_{\mathrm{quartz}}(\omega_{\mathrm{VIS}}) r_{\mathrm{quartz}}(\omega_{\mathrm{IR}}) E_{\mathrm{VIS}}E_{\mathrm{IR}}|^2\\ &\qquad + |r_{\mathrm{GaAs}}\varepsilon_0 F_{\mathrm{quartz}}\chi^{(2)}_{\mathrm{quartz}} E_{\mathrm{VIS}}E_{\mathrm{IR}}|^2 \qquad (19)\end{aligned}$$

In this case we have to use the fact that the second term is equal to the direct SFG reference. Subtracting this term and dividing eq 18 by the resulting expressions gives

$$\begin{aligned}\frac{|E_{\mathrm{LO,s}}|^2}{|E_{\mathrm{LO,q}}|^2} &= \frac{|\varepsilon_0 F_{\mathrm{GaAs}}\chi^{(2)}_{\mathrm{GaAs}} r_{\mathrm{sample}}(\omega_{\mathrm{VIS}}) r_{\mathrm{sample}}(\omega_{\mathrm{IR}}) E_{\mathrm{VIS}}E_{\mathrm{IR}}|^2}{|\varepsilon_0 F_{\mathrm{GaAs}}\chi^{(2)}_{\mathrm{GaAs}} r_{\mathrm{quartz}}(\omega_{\mathrm{VIS}}) r_{\mathrm{quartz}}(\omega_{\mathrm{IR}}) E_{\mathrm{VIS}}E_{\mathrm{IR}}|^2}\\ &= \frac{|r_{\mathrm{sample}}(\omega_{\mathrm{VIS}}) r_{\mathrm{sample}}(\omega_{\mathrm{IR}})|^2}{|r_{\mathrm{quartz}}(\omega_{\mathrm{VIS}}) r_{\mathrm{quartz}}(\omega_{\mathrm{IR}})|^2} \qquad (20)\end{aligned}$$

which is exactly the correction term we were looking for (see eq 11). Figure 9 shows the correction extracted in this way compared to the squared magnitude of the complex reflectivity of water with an incident angle of 40°.

## REFERENCES


(1) Eisenthal, K. B. *Chem. Rev.* **1996**, *96*, 1343.
(2) Shen, Y. R. *Solid State Commun.* **1997**, *102*, 221.
(3) Allen, H. C.; Raymond, E. A.; Richmond, G. L. *Curr. Opin. Colloid Interface Sci.* **2000**, *5*, 74.
(4) Vidal, F.; Tadjeddine, A. *Rep. Prog. Phys.* **2005**, *68*, 1095.
(5) Gopalakrishnan, S.; Liu, D.; Allen, H. C.; Kuo, M.; Shultz, M. J. *Chem. Rev.* **2006**, *106*, 1155.
(6) Aliaga, C.; Santos, C. S.; Baldelli, S. *Phys. Chem. Chem. Phys.* **2007**, *9*, 3683.
(7) Yamaguchi, S.; Tahara, T. *Laser Photonics Rev.* **2008**, *2*, 74.
(8) Somorjai, G. A.; Frei, H.; Park, J. Y. *J. Am. Chem. Soc.* **2009**, *131*, 16589.
(9) Arnolds, H.; Bonn, M. *Surf. Sci. Rep.* **2010**, *65*, 45.
(10) Feng, R.-r.; Guo, Y.; Lue, R.; Velarde, L.; Wang, H.-f. *J. Phys. Chem. A* **2011**, *115*, 6015.
(11) Ostroverkhov, V.; Waychunas, G. A.; Shen, Y. R. *Phys. Rev. Lett.* **2005**, *94*.
(12) Stiopkin, I. V.; Jayathilake, H. D.; Bordenyuk, A. N.; Benderskii, A. V. *J. Am. Chem. Soc.* **2008**, *130*, 2271.
(13) Nihonyanagi, S.; Yamaguchi, S.; Tahara, T. *J. Chem. Phys.* **2009**, *130*.
(14) Chen, X.; Hua, W.; Huang, Z.; Allen, H. C. *J. Am. Chem. Soc.* **2010**, *132*, 11336.
(15) Shen, Y. R.; Ostroverkhov, V. *Chem. Rev.* **2006**, *106*, 1140.
(16) Mondal, J. A.; Nihonyanagi, S.; Yamaguchi, S.; Tahara, T. *J. Am. Chem. Soc.* **2010**, *132*, 10656.
(17) Laaser, J. E.; Xiong, W.; Zanni, M. T. *J. Phys. Chem. B* **2011**, *115*, 2536.
(18) Lambert, A. G.; Davies, P. B.; Neivandt, D. J. *Appl. Spectrosc. Rev.* **2005**, *40*, 103.
(19) Bloembergen, N.; Pershan, P. S. *Phys. Rev.* **1962**, *128*, 606.
(20) Kemnitz, K.; Bhattacharyya, K.; Hicks, J. M.; Pinto, G. R.; Eisenthal, B.; Heinz, T. F. *Chem. Phys. Lett.* **1986**, *131*, 285.
(21) Lu, R.; Rao, Y.; Zhang, W. K.; Wang, H. F. "Phase measurement in nonlinear optics of molecules at air/water interface with femtosecond laser pulses"; Proceedings of SPIE - The International Society for Optical Engineering, 2002.
(22) Auer, B. M.; Skinner, J. L. *J. Phys. Chem. B* **2009**, *113*, 4125.
(23) Jung, L. S.; Campbell, C. T.; Chinowsky, T. M.; Mar, M. N.; Yee, S. S. *Langmuir* **1998**, *14*, 5636.
(24) Griffiths, D. J. *Introduction to Electrodynamics*, 3rd ed.; Prentice Hall: Upper Saddle River, NJ, 1999.
(25) Querry, M. R.; Wieliczka, D. M.; Segelstein, D. J. *Handbook of Optical Constants of Solids*, 1st ed.; Academic Press: Waltham, MA, 1991; Vol. 2.
(26) Watry, M. R.; Tarbuck, T. L.; Richmond, G. I. *J. Phys. Chem. B* **2003**, *107*, 512.
(27) Watanabe, K.; Inoue, K.; Nakai, I. F.; Matsumoto, Y. *Phys. Rev. B* **2010**, *81*, 4.
(28) Dadap, J. I.; Shan, J.; Weling, A. S.; Misewich, J. A.; Heinz, T. F. *Appl. Phys. B* **1999**, *68*, 333.